Journal of Materials Chemistry

Cite this: J. Mater. Chem., 2012, 22, 18847

www.rsc.org/materials

PAPER

Novel approach toward a binder-free and current collector-free anode configuration: highly flexible nanoporous carbon nanotube electrodes with strong mechanical strength harvesting improved lithium storage†

Xifei Li,[a] Jinli Yang,[a] Yuhai Hu,[a] Jiajun Wang,[a] Yongliang Li,[a] Mei Cai,[b] Ruying Li[a] and Xueliang Sun*[a]

Received 23rd May 2012, Accepted 5th July 2012
DOI: 10.1039/c2jm33297c

In this work, we developed a novel flexible nanoporous carbon nanotube film to use as a binder-free and current collector-free anode electrode for lithium ion batteries, providing a new approach to flexible energy devices. The proposed novel anode configuration shows better cycling performance and rate capability than the conventional electrode architecture. Moreover, this unique configuration exhibits good flexibility and robust mechanical strength, which has the potential to be applied to flexible lithium ion batteries. Our findings may provide a new anode configuration for lithium ion batteries with improved cycling stability and rate capability.

1. Introduction

The hybrid electric vehicle (HEV) and plug-in hybrid electric vehicle (PHEV) technology with enormous potential for low- or zero-emission has been the impetus for the research and development of high performance lithium ion batteries (LIBs). Increasing the energy density of LIBs is an attractive route for their possible application to HEVs and PHEVs. Recently, some new promising anode materials, such as Si (4200 mA h g^{-1}) and Sn (994 mA h g^{-1}) with much higher theoretical capacities than the commercialized graphite anode, have attracted tremendous interest in the effort to achieve high energy density in LIBs.[1–3] Unfortunately, the poor cyclability caused by the large volume change during alloying/de-alloying with lithium severely prevents their commercialization.[4–7] Conventional methods for the fabrication of LIB electrodes usually involve mixing, casting, and pressing the mixed constituents, including a cathode or an anode for lithium storage, a binder, such as polyvinylidene fluoride, to inhibit the collapse of the active materials from metal current collectors, and an electrical conductor to maintain the electrode conductivity onto the metal current collectors.[8–10] It is worth noting that the binders and the metal current collectors make no contribution to lithium storage, and the electrical conductor exhibits minimal lithium storage performance; thus, these components significantly decrease the energy density of LIBs. Moreover, the presence of binders in the electrodes decreases the accessible specific area of the active materials and increases the electrochemical polarization of the electrodes, undermining effective lithium ion transport. From the perspective of optimal performance, the optimization of the electrode system may increase the energy density of LIBs, for example, by decreasing the dosage of the binder, the electrical conductor and the current collector.[11] In particular, binder-free, electrical conductor-free and current collector-free configurations can effectively satisfy this goal.[12] Meanwhile, the investigation and development of flexible power sources are also motivated by the numerous potential applications of flexible and wearable electronic devices.[13] In a commercialized LIB, both electrodes are based on metal current collectors, which are not flexibly bendable because the active material layers are easily cracked or peeled off when metal current collectors are bent.[14] As a result, the development of a flexible, lightweight, and environmentally benign binder-free and current collector-free electrode configuration to increase the energy density of LIBs has drawn some research attention.[15–17] For example, graphene thin films have been fabricated as anode electrodes for LIBs.[17] However, to the best of our knowledge, most previously reported flexible thin film electrodes without a supporting substrate exhibit limited mechanical strength, which has been a crucial challenge in LIB applications.

Carbon nanotubes (CNTs) with advantageous electrical properties, high mechanical strength, great chemical stability, high aspect ratios, and large activated surface areas[18,19] have been the focus of both fundamental science and applied research since their discovery in 1991.[20–23] The lithium storage capacity of CNTs results from the effective diffusion of lithium ions into stable sites located on the nanotube surface and inside individual nanotubes through endcap and sidewall openings, as well as between CNT layers.[24,25] Shao-Horn *et al.* created binder-free and self-standing oxidized few-walled CNTs as cathode electrodes, which exhibited high power density and high

[a]*Department of Mechanical and Materials Engineering, University of Western Ontario, London, Ontario, N6A 5B9, Canada. E-mail: xsun@eng.uwo.ca; Fax: +1 519 661 3020; Tel: +1 519 661 2111 ext. 87759*
[b]*General Motors R&D Center, Warren, MI 48090-9055, USA*
† Electronic supplementary information (ESI) available. See DOI: 10.1039/c2jm33297c

energy density (a high gravimetric energy of approximately 200 W h kg^{-1} at a high power of 10 kW kg^{-1}) as a result of the combination of chemical redox reactions and high surface area capacitive storage.[26] Novak's research group reported conductive CNT films with 10 wt% carbon black that were used as binder-free and current-free anode electrodes for LIBs.[16] However, the inevitable voids among the CNTs in the resultant electrodes greatly decrease their mechanical strength. The loss of mechanical strength makes the use of these binder-free and current collector-free electrodes difficult in practical LIB applications.

In this investigation, we will demonstrate a simple and convenient route to directly fabricate CNT anode films on the commercially used separators in LIBs. By combining CNT thin films with the separators, this system provides inherent flexibility and porosity. The existence of the separators significantly increases the mechanical strength of the anode electrodes. As a result, in comparison to CNT anodes on copper substrates (CNTs-Cu), the obtained binder-free and current collector-free electrodes are sufficiently lightweight and flexible to be rolled up or twisted, and can be manufactured at low cost with improved energy density for LIBs.

2. Experimental section

Synthesis of CNTs-separator and CNTs-Cu

Commercial carbon nanotubes (CNTs) from Shenzhen Nanotech Port Co., Ltd were used as received, without further purification. In a typical procedure, the CNTs (100 mg), with a diameter of 15–60 nm and a length of 1–6 μm, were dispersed in deionized water (DI water, 100 mL) with Triton X-100 (1 mL) as the surfactant to form a suspension under an ultrasonic force. The obtained suspension was purified by a centrifuge treatment to remove impurities and carbon particles. A vacuum filtration method was employed to obtain CNT films on Celgard 3500 as the LIB polypropylene separator (CNTs-separator). The as-prepared suspension was filtered through a porous filter paper, the Celgard 3500 polypropylene separator. As the solvent went through Celgard 3500, the CNTs were trapped on the surface, forming an entangled CNT film on Celgard 3500. After that, the resultant CNT films were washed with DI water (1600 mL), followed by methanol (100 mL) to remove any remaining surfactant residue. Subsequently, CNTs-separator was dried in a vacuum chamber at 80 °C for 72 h.

The CNTs-Cu electrode was prepared using commercial carbon nanotubes derived from slurry casting on a Cu foil as the commercial current collector for LIBs. The slurry contained commercial CNTs (90 wt% on dry solids basis) and a polyvinylidene fluoride binder (10 wt% on dry solids basis) in *N*-methylpyrrolidinone (NMP) solvent. The electrodes were dried in a vacuum oven at 90 °C overnight.

Characterization of CNTs-separator and CNTs-Cu

The morphologies of CNTs-separator and CNTs-Cu were examined in a field emission scanning electron microscope (FE-SEM, Hitachi S-4800), transmission electron microscope (TEM, Hitachi H-7000), and high-resolution transmission electron microscope (HRTEM, JEOL 2010F). Powder X-ray diffraction (XRD) patterns were recorded by a Rigaku RU-200BVH diffractometer employing a Co-K_α source (λ = 1.7892 Å). Raman spectra were obtained using a HORIBA Scientific Lab-RAM HR Raman spectrometer system equipped with a 532.4 nm laser as the exciting radiation equipped with an optical microscope at room temperature.

Electrochemical lithium storage behavior

A coin-type electrochemical half-cell included a prepared electrode as the working electrode and a lithium foil as the counter electrode (CNTs-Cu with a polypropylene separator (Celgard 3500), CNTs-separator without Celgard 3500). The electrolyte was composed of 1 M $LiPF_6$ salt dissolved in ethylene carbonate (EC) : diethyl carbonate (DEC) : ethyl methyl carbonate (EMC) in a 1 : 1 : 1 volume ratio. CR-2016-type coin cells were assembled in a glove box under a dry argon atmosphere (moisture and oxygen concentration <1 ppm). Cyclic voltammetry (CV) and the electrochemical impedance spectra (EIS) tests were performed on a versatile multichannel potentiostat 3/Z (VMP3) at a scan rate of 0.1 mV s^{-1} over a potential range of 0.01 to 3.0 V (*vs.* Li/Li^+). Charge–discharge characteristics were tested galvanostatically between 0.01 and 3.0 V (*vs.* Li/Li^+) at room temperature using an Arbin BT-2000 Battery Tester.

3. Results and discussion

The morphologies of the CNTs and CNTs-separator were examined by SEM and HRTEM, as shown in Fig. 1. The inset of Fig. 1a is a FE-SEM image of the CNTs at low magnification

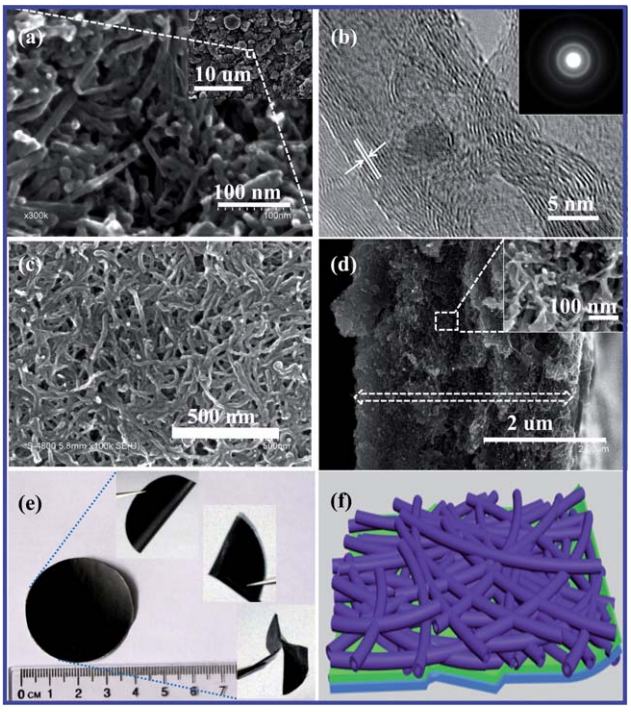

Fig. 1 (a) SEM and (b) HRTEM (SAED in the inset) images of CNTs; (c) SEM and (d) cross-sectional image of CNTs-S; (e) digital optical image of a highly flexible CNTs-S folded and rolled up; and (f) schematic diagram of a binder-free and current collector-free anode configuration.

which indicates that the interconnected CNTs are sticking together to form agglomerates. The increased magnification in Fig. 1a also reveals that the CNTs have a wide range of external diameters (15–60 nm). The typical HRTEM image in Fig. 1b shows that the aligned CNTs are graphitized carbon and typically consist of approximately 14 layers with a spacing of 0.34 nm, which closely corresponds to the interplanar distance of the (002) plane of CNTs.[27,28] The selected area electron diffraction (SAED) pattern obtained for the CNTs is shown in the inset of Fig. 1b. The pattern displays obvious diffraction rings produced by cylindrical graphite sheets.[29,30] A top-view SEM image of CNTs-separator is shown in Fig. 1c. As the image shows, the CNTs are formed into tangled, dense, and homogeneous electrically conductive networks with a typical diameter of 15–20 nm. Interestingly, the randomly oriented individual CNTs form an interconnected nanoporous structure that plays an important role in the path of the transportation of ions between the electrolytes and the active materials. The cross-sectional image of CNTs-separator in Fig. 1d clearly shows that the CNT electrode formed on Celgard 3500 has a thickness of approximately 3.7 μm. Fig. 1e presents photographs of CNTs-separator with an area of 12 cm^2 and photographs of CNTs-separator folded in half, in quarters, and to 1/16. Visual evidence of the mechanical strength is illustrated in Fig. 1e, which shows that the CNTs-separator can be flexibly rolled up, twisted, and bent to many curvatures without any unintended or irreversible deformation, suggesting that CNTs-separator can be shaped into any form factor required and cut easily with conventional cutters or shears. The ultrasonic impact treatments were performed on CNTs-Cu and CNTs-separator in order to further demonstrate the strong mechanical strength of CNTs-separator. CNTs-Cu and CNTs-separator with a diameter of 9/16 inch were treated in alcohol by ultrasonication. It is obvious that the suspension color of CNTs-Cu was totally changed to black because most of the CNT powders were removed from the Cu foil as shown in Fig. S1a,† but almost no color change was observed for CNTs-separator (see Fig. S1b†), which indicates that CNTs-separator is capable of exhibiting strong mechanical strength.

It is well known that a vacuum filtration approach has been widely employed to prepare CNT films.[16,31] As previously reported,[16] the CNT film can be formed on the PVDF membrane *via* a vacuum filtration method. Then the CNT film was peeled off from the PVDF membrane, and a free-standing CNT film was successfully synthesized. However, as we mentioned in the Introduction section, the inevitable voids among the CNTs in the resultant films greatly decrease the mechanical strength. For example, when we rolled up and folded a free-standing CNT film synthesized by a vacuum filtration approach, some obvious and severe cracks were observed as shown in Fig. S2.† The processing steps of the LIB fabrication utilize roll coaters or die cutting; thus, the mechanical strength is an important consideration for CNT film electrodes because binders and metal current collectors are absent.[32] The loss of mechanical strength of the CNT film by traditional vacuum filtration makes the use of these binder-free and current collector-free electrodes difficult in practical LIB applications. Therefore, good flexibility and robust mechanical strength of the CNTs-separator provide the possibility that the anode electrode could be used in flexible electronic devices.

The resultant CNTs-Cu and CNTs-separator were characterized by XRD, as shown in Fig. 2a. The diffraction peaks corresponding to Celgard 3500 and the Cu foil are marked by a square and a circle, respectively. Both spectra show a peak positioned at 30.3°, which is indexed readily to the (002) graphite plane in the CNTs.[33,34] However, CNTs-separator exhibits a much stronger diffraction peak than CNTs-Cu, although the CNT loading amount is similar on both electrodes. The Raman spectra of CNTs-Cu and CNTs-separator are given in Fig. 2b for comparison. Both spectra show three obvious peaks: the G band with E_{2g} symmetry at approximately 1567 cm^{-1}, the D band with A_{1g} symmetry at approximately 1330 cm^{-1} and the 2D band at approximately 2665 cm^{-1}.[35] The integrated intensity ratio of the D band and the G band (I_D/I_G) is a critical factor for measurement of the disorder degree of carbon nanotubes to compare structural changes.[36–39] The I_D/I_G values of CNTs-Cu and CNTs-separator are 0.46 and 0.36, respectively. Our Raman spectroscopy analysis shows that I_D/I_G decreased slightly after the ultrasonication and centrifugation treatment of the carbon nanotubes, which indicates that some carbon nanotubes with a low graphitic nature were removed during the centrifugation process. In comparison with the low graphitic ones, the high graphitic carbon nanotubes exhibit higher electrical conductivity, which is beneficial for Li^+ intercalation/de-intercalation into the anodes.[40]

The EIS were tested at the voltage of 0.05 V in the fifth discharge. Fig. 3 shows the EIS of CNTs-Cu and CNTs-separator, respectively. Clearly, the impedance value of CNTs-Cu is higher than that of CNTs-separator. A possible equivalent circuit is depicted in the inset of Fig. 3. R_e is the electrolyte ohmic resistance, while R_{sl} corresponds to the resistance for Li^+ migration through the SEI film, and C_{sl} denotes the interfacial capacitance corresponding to R_{sl}. C_{dl} and R_{ct} are the double-layer capacitance and the charge transfer resistance, respectively. W is the finite length Warburg impedance that reflects the solid-state diffusion in the anodes.[41,42] After simulation by the equivalent circuit, it is found that the charge transfer resistance of CNTs-Cu and CNTs-separator is 216 Ω and 157 Ω, respectively. CNTs-Cu includes an additional binder with poor electrical conductivity, showing higher resistance in comparison to CNTs-separator.

Fig. 4a and b show typical CV profiles of CNTs-Cu and CNTs-separator, respectively. During the first cathodic scan, CNTs-Cu produces a dominant cathodic peak at approximately 0.61 V that is attributed to the formation of a solid electrolyte interphase (SEI) on the anode surface, which is not followed by any peak from the second cathodic scan. The peak close to 0 V corresponds to lithium intercalation into the CNTs.[40] The anodic peak at 0.25 V is produced by lithium de-intercalation from the anode. However, CNTs-separator exhibits different behavior in the SEI system. The formation peak of CNTs-separator can be observed at approximately 0.72 V in the first cathodic scan. Interestingly, in the subsequent scan, the peaks at 0.76 V indicate the partly reversible SEI process on the anode. The partially reversible formation/decomposition of the SEI is beneficial providing extra reversible energy capacity.[43] Some oxygen-containing surface groups are inevitably formed on the surface of the commercial CNTs. As a result, both anodes show small cathodic peaks around 1.1 V due to the reduction processes, which result from

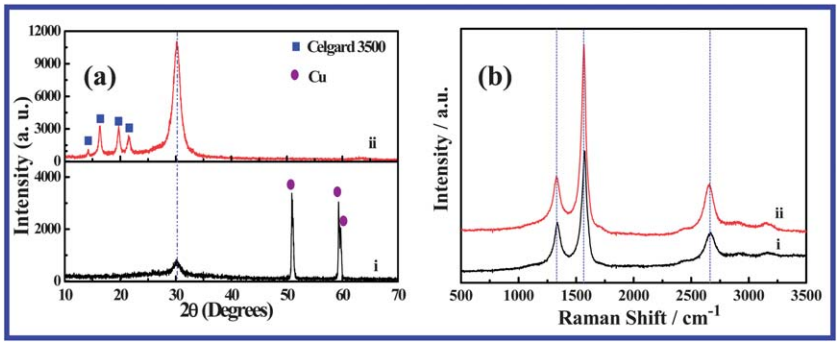

Fig. 2 (a) X-ray diffraction and (b) Raman spectra of (i) CNTs-C and (ii) CNTs-S.

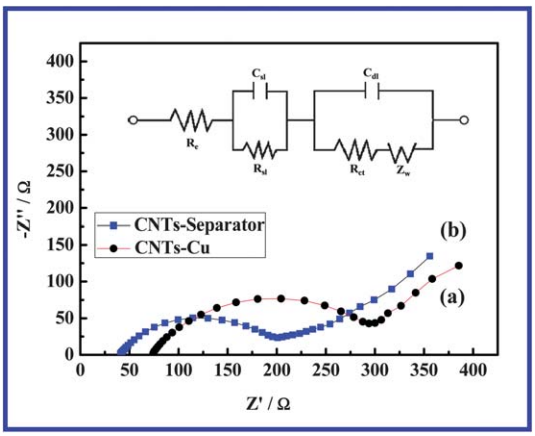

Fig. 3 Electrochemical impedance spectra of (a) CNTs-Cu and (b) CNTs-separator at 0.05 V in the fifth discharge; the inset is the equivalent circuit to fit the EIS.

the reduction of the oxygen-containing surface species in the lateral defect sites and maybe in the grain boundaries.[44]

Galvanostatic charge–discharge tests were employed to study the lithium intercalation/de-intercalation behavior of CNTs-Cu and CNTs-separator (see Fig. 4c and d). Both electrodes exhibit similar lithium storage behavior. But they show different open circuit voltages (OCV), which may be due to the different Fermi levels of CNTs-Cu and CNTs-separator.[44] CNTs-Cu has specific capacities of 768 and 237 mA h g^{-1} for the discharge and charge processes in the first cycle, respectively, while CNTs-separator has values of 863 and 281 mA h g^{-1}, respectively. During the second discharge, the specific capacities of CNTs-Cu and CNTs-separator decrease to 277 and 332 mA h g^{-1}, and the capacity fade is 64% and 62% in comparison to the value in the first discharge, respectively. The low capacity retention is due to the highly irreversible behavior in the first cycle, but the small difference in the capacity fade results from different electrical conductivities and average diameters, SEI reversibility of

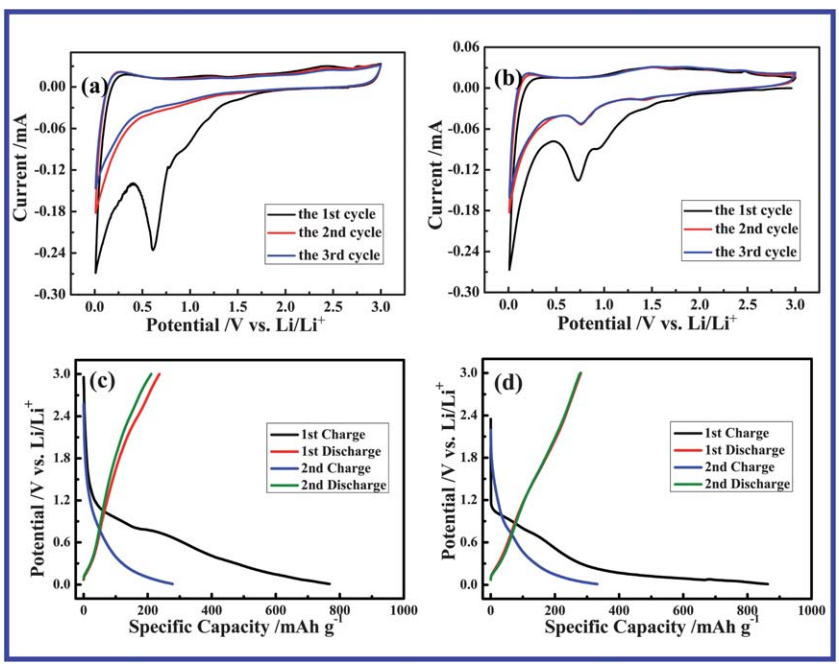

Fig. 4 Cyclic voltammograms of (a) CNTs-C and (b) CNTs-S as anodes at a scan rate of 0.1 mV s^{-1} in a voltage range of 0.01–3.00 V; charge–discharge profiles of (c) CNTs-C and (d) CNTs-S at a current density of 100 mA g^{-1}.

CNTs-Cu and CNTs-separator. Clearly, the CNTs-separator electrode exhibits higher reversible energy capacity than the conventional electrode with CNTs casting on a Cu foil.

The cycling performance of CNTs-Cu and CNTs-separator electrodes at a current density of 100 mA g^{-1} is shown in Fig. 5a. CNTs-separator clearly exhibits a higher specific energy capacity than CNTs-Cu throughout the first 100 cycles. In particular, the cyclability of the CNTs-Cu electrode is much poorer. The discharge capacity retention after 100 cycles is only 42% of its value during the second cycle, whereas a significant improvement can be observed in the CNTs-separator electrode (76% capacity retention after 100 cycles). When the current density applied to the CNTs-separator electrode was decreased from 100 to 50 mA g^{-1}, an improved reversible capacity of 375 mA h g^{-1} was obtained in the second discharge, and a capacity retention of 80% was obtained after 100 cycles. It was reported that the film thickness has a strong effect on the electrochemical performance of the anodes,[45–49] for example, the Si thin films of 250 nm and 1.0 μm dimensions sputter deposited on a Cu foil substrate yielded reversible capacities of 3500 and 3000 mA h g^{-1} at a rate of 0.4 C, respectively.[45] In a vacuum filtration process, the thickness of the obtained CNT film on the separator strongly depends on the suspension volume used, which indicates that the proposed anode configuration in this research has a significant advantage of accurate control of the anode thickness. The CNTs-separator anodes with different thicknesses were synthesized, and three thicknesses (1.0, 3.7, and 6.1 μm) were verified by cross-sectional SEM images, as shown in Fig. S3a–c.† The effect of thickness on the electrochemical performance of CNTs-separator is displayed in Fig. S4b.† As expected, one can see that the thickness of the CNTs-separator anodes can significantly affect the specific capacity. The 1.0 μm film exhibits the highest reversible capacity of 416 mA h g^{-1}. However, the increase in thickness from 1.0 μm to 6.1 μm results in obvious capacity decrease. The CNTs-separator anodes with different thicknesses show different adhesions to the separator.[45] Moreover, aggregation together with SEI layer formation results in increased diffusion length as the film thickness increases.[48] As a result, the thickness of CNTs-separator has a significant influence on the specific capacity.

Fig. 5b shows that both electrodes with high irreversible capacities show low coulombic efficiency in the initial cycle, which is a result of electrolyte reduction and SEI formation, as shown in the CV curves in Fig. 4a and b. In the subsequent cycles, the coulombic efficiencies of both CNTs-Cu and CNTs-separator undergo an obvious increase. Moreover, the coulombic efficiency of CNTs-separator reaches nearly 100% after 15 charge–discharge cycles. Importantly, CNTs-separator exhibits higher coulombic efficiency than CNTs-Cu, which indicates a remarkable decrease of the irreversible capacity loss during the charge–discharge processes.

The good cycling performance of CNTs-separator motivates us to test its rate capability, which is an important parameter of LIBs for many applications that require fast charge and discharge rates.[50] Fig. 5c and d show the rate capability of CNTs-Cu and the CNTs-separator electrodes as a function of current density from 100 to 1200 mA g^{-1}. In comparison to CNTs-Cu, the CNTs-separator anode exhibits higher and steadier capacities, even at a high current density of 1200 mA g^{-1} (see Fig. 5c). The charge–discharge capacities can be observed to decrease as the current density increases; this decrease is attributed to the anode overpotential caused by the limited lithium diffusion

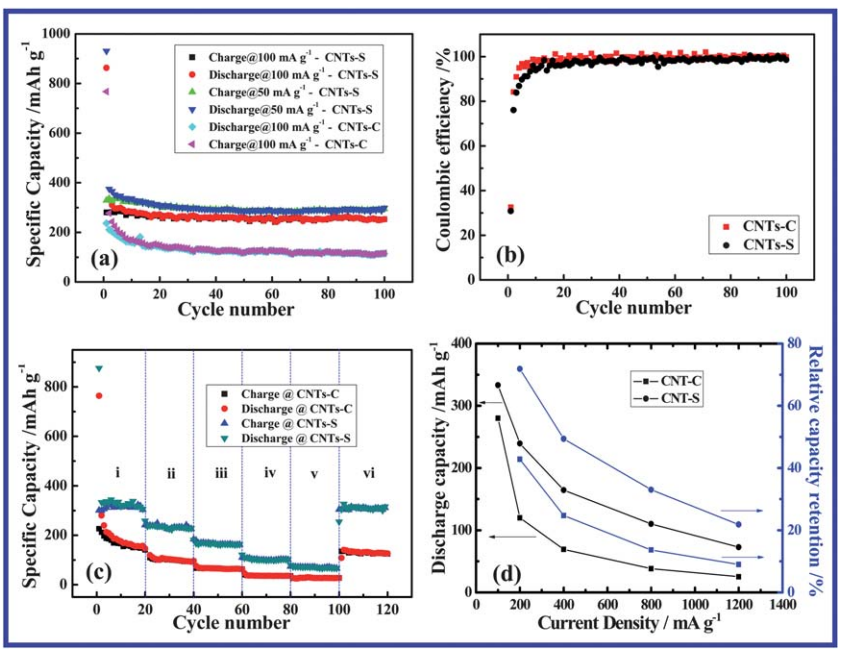

Fig. 5 (a) Reversible charge–discharge capacity *versus* cycle numbers of CNTs-C and CNTs-S at a current density of 50 and 100 mA g^{-1}; (b) coulombic efficiency of CNTs-C and CNTs-S at a current density of 100 mA g^{-1}; (c) rate capability of CNTs-C and CNTs-S at various current densities: (i) 100, (ii) 200, (iii) 400, (iv) 800, (v) 1200, and (vi) 100 mA g^{-1}; (d) discharge capacities of CNTs-C and CNTs-S at the second cycle as a function of current density from 100 mA g^{-1} to 1200 mA g^{-1}, and relative capacity retention at 200, 400, 800, and 1200 mA g^{-1} in comparison to the discharge capacity at 100 mA g^{-1}.

kinetics.[40,51] However, as shown in Fig. 5d, the CNTs-separator anode is capable of showing higher energy capacities than CNTs-Cu at every current density. Moreover, the decrease in the specific capacity is lower for CNTs-separator than for CNTs-Cu. The discharge capacities of the second cycle at various current densities are compared with the capacity at 100 mA g^{-1} in Fig. 5d. The CNTs-separator anode was found to maintain greater capacity retention at 200 mA g^{-1}, 400 mA g^{-1}, 800 mA g^{-1} and 1200 mA g^{-1} than the CNTs-Cu anode. Consequently, the CNTs-separator anode demonstrated better rate capability than CNTs-Cu as an anode for LIBs.

The conventional electrode process involves mixing the CNTs, the electronic conductor (typically 10–15% acetylene black by weight or volume) and the binder (typically 5–10% poly-(vinylidene fluoride) by weight or volume) with *n*-methyl-2-pyrrolidone solvent and coating the resultant slurry on the copper foil as a current collector.[50,52] Characterized by their cycling performance and rate capability, the battery performance of the obtained CNT electrodes in all references is not satisfactory, which might be caused by the lack of superior conductive paths.[53] In this study, however, the complex steps in conventional processing can be simplified by using highly flexible binder-free and current collector-free electrodes with robust mechanical strength (see Fig. 1f). First, the absence of the binder is beneficial due to the increased electrical conductivity of the electrodes. Second, the binder can initiate exothermic reactions and lead to potential explosions and, as a result, the binder-free system can increase LIB abuse tolerance.[54] Third, examination of the morphology of CNTs-separator was performed by SEM after charge–discharge cycles. It can be observed that the dense CNTs are still tangled together (Fig. S4a†). The ultrasonic treatment (see Fig. S4b†) of the cycled CNTs-separator indicates that after charge–discharge cycles the CNT film can still maintain tight contact with the separator, resulting from the strong adhesion of the CNT film to the separator. CNTs-separator is more stable, increasing the structural stability during the charge–discharge process because of the strong adhesion of the CNT film to Celgard 3500.[55,56] Fourth, the nanoporous CNT electrodes provide a super-accessible contact area with the electrolyte, permitting higher concentrations of lithium ion intercalation–de-intercalation to occur during the charge–discharge processes.[57] Fifth, CNTs-separator provides a more developed nanoporous structure and conductive pathway, making it more effective for electrode construction.[53] Sixth, some of the catalyst attached to the surface of the CNTs can be removed during the ultrasonication and centrifugation processes to improve the battery performance of the anodes. Another advantage of the proposed anode configuration is its accurate control of the anode thickness, which is a desired feature when sizing an anode to exactly match with a cathode for higher energy density LIB.[58] All of these benefits endow the proposed binder-free and current collector-free anode configuration with significantly improved cycling performance and rate capability. Moreover, the binder-free and current collector-free system contributes to the increased energy density of the LIBs because it lacks binders and current collectors.[52,59]

It is worth noting that Lee *et al.* synthesized a CNT anode with a diameter of 20–40 nm by chemical vapor deposition at 750 °C, and they obtained an initial reversible capacity of ~200 mA h g^{-1},[60] which is close to that of the commercial CNTs used in this research. However, our novel anode configuration exhibits an obvious advantage of increased specific capacity up to 378 mA h g^{-1}. In order to fulfill the requirement of high energy capacity, Lee *et al.* introduced Sb and $SnSb_{0.5}$ anodes with high energy capacities in the CNTs, where a high capacity of 518 mA h g^{-1} can be obtained.[60] Similarly, the higher capacity can be expected to be achieved if some anodes, such as Sn and Si, are added into our novel anode configuration although it is not a focus of this research. How to create CNTs-separator based composite anode configuration is our future research work.

4. Conclusion

In summary, we have proposed and realized an effective approach to obtain a binder-free and current collector-free nanoporous carbon nanotube film on the separator as a LIB anode electrode to create flexible energy devices. The existence of the separator does not decrease the energy density because it is an important and necessary component of the LIB system. More importantly, the separator used as the supporter in the proposed highly flexible electrode guarantees high mechanical strength, enabling its practical application to LIBs. We demonstrated that these highly flexible electrodes can significantly improve lithium storage in comparison to the CNT-Cu electrodes. The battery without a binder or a current collector can effectively decrease the weight of the LIB system and enhance the energy density of the LIBs. The current approach also works for other anode materials in LIBs. This new anode configuration will increase the LIB energy density and may have promising applications in flexible LIBs. Additionally, this configuration opens the door for potentially satisfying the requirements of various flexible and lightweight electronic devices.

Acknowledgements

This research was supported by the Natural Science and Engineering Research Council of Canada (NSERC), General Motors of Canada, Canada Research Chair (CRC) Program, Canadian Foundation for Innovation (CFI), Ontario Research Fund (ORF), Early Researcher Award (ERA) and the University of Western Ontario. The authors are in debt to Dr. Yong Zhang for his kind help on drawing. X. Li is grateful to Springpower International, Inc. and the MITACS Elevate Strategic Fellowship Program.

References

1 A. Magasinki, P. Dixon, B. Hertzberg, A. Kvit, J. Ayala and G. Yushin, *Nat. Mater.*, 2010, **9**, 353–358.
2 H. Ma, F. Cheng, J. Y. Chen, J. Z. Zhao, C. S. Li, Z. L. Tao and J. Liang, *Adv. Mater.*, 2007, **19**, 4067–4070.
3 W. M. Zhang, J. S. Hu, Y. G. Guo, S. F. Zheng, L. S. Zhong, W. G. Song and L. J. Wan, *Adv. Mater.*, 2008, **20**, 1160–1165.
4 C. K. Chan, H. Peng, G. Liu, K. McIlwrath, X. F. Zhang, R. A. Huggins and Y. Cui, *Nat. Nanotechnol.*, 2008, **3**, 31–35.
5 X. F. Li, A. Dhanabalan and C. L. Wang, *Adv. Energy Mater.*, 2012, **2**, 238–244.
6 J. R. Szczech and S. Jin, *Energy Environ. Sci.*, 2011, **4**, 56–72.
7 X. F. Li, X. B. Meng, J. Liu, D. S. Geng, Y. Zhang, M. Banis, Y. L. Li, J. L. Yang, R. Y. Li, X. L. Sun, M. Cai and M. Verbrugge, *Adv. Funct. Mater.*, 2012, **22**, 1647–1654.
8 Y. Idota, T. Kubota, A. Matsufuji, Y. Maekawa and T. Miyasaka, *Science*, 1997, **276**, 1395–1397.

9 X. F. Li, D. S. Geng, Y. Zhang, X. b. Meng, R. y. Li and X. L. Sun, *Electrochem. Commun.*, 2011, **13**, 822–825.
10 X. F. Li and C. L. Wang, *RSC Adv.*, 2012, **2**, 6150–6154.
11 M. S. Whittingham, *Chem. Rev.*, 2004, **104**, 4271–4302.
12 R. A. DiLeo, S. Frisco, M. J. Ganter, R. E. Rogers, R. P. Raffaelle and B. J. Landi, *J. Phys. Chem. C*, 2011, **115**, 22609–22614.
13 M. Peckerar, Z. Dilli, M. Dornajafi, N. Goldsman, Y. Ngu, R. B. Proctor, B. J. Krupsaw and D. A. Lowy, *Energy Environ. Sci.*, 2011, **4**, 1807–1812.
14 J. Z. Wang, S. L. Chou, H. Liu, G. X. Wang, C. Zhong, S. Y. Chew and H. K. Liu, *Mater. Lett.*, 2009, **63**, 2352–2354.
15 A. Patil, V. Patil, D. W. Shin, J. W. Choi, D. S. Paik and S. J. Yoon, *Mater. Res. Bull.*, 2008, **43**, 1913–1942.
16 S. Y. Chew, S. H. Ng, J. Z. Wang, P. Novak, F. Krumeich, S. L. Chou, J. Chen and H. K. Liu, *Carbon*, 2009, **47**, 2976–2983.
17 H. Gwon, H. S. Kim, K. U. Lee, D. H. Seo, Y. C. Park, Y. S. Lee, B. T. Ahn and K. Kang, *Energy Environ. Sci.*, 2011, **4**, 1277–1283.
18 H. Dai, *Surf. Sci.*, 2002, **500**, 218–241.
19 K. P. Gong, F. Du, Z. H. Xia, M. Durstock and L. M. Dai, *Science*, 2009, **323**, 760–764.
20 S. Iijima, *Nature*, 1991, **354**, 56–58.
21 A. Thess, R. Lee, P. Nikolaev, H. J. Dai, P. Petit, J. Robert, C. H. Xu, Y. H. Lee, S. G. Kim, A. G. Rinzler, D. T. Colbert, G. E. Scuseria, D. Tomanek, J. E. Fischer and R. E. Smalley, *Science*, 1996, **273**, 483–487.
22 M. M. J. Treacy, T. W. Ebbesen and J. M. Gibso, *Nature*, 1996, **381**, 678–680.
23 R. H. Baughman, A. A. Zakhidov and W. A. de Heer, *Science*, 2002, **297**, 787–792.
24 B. J. Landi, M. J. Ganter, C. D. Cress, R. A. DiLeo and R. P. Raffaelle, *Energy Environ. Sci.*, 2009, **2**, 638–654.
25 B. Song, J. W. Yang, J. J. Zhao and H. P. Fang, *Energy Environ. Sci.*, 2011, **4**, 1379–1384.
26 S. W. Lee, B. M. Gallant, Y. Lee, N. Yoshida, D. Y. Kim, Y. Yamada, S. Noda, A. Yamada and Y. Shao-Horn, *Energy Environ. Sci.*, 2012, **5**, 5437–5444.
27 G. F. Zou, H. M. Luo, S. Baily, Y. Y. Zhang, N. F. Haberkorn, J. Xiong, E. Bauer, T. M. McCleskey, A. K. Burrell, L. Civale, Y. T. Zhu, J. L. MacManus-Driscoll and Q. X. Jia, *Nat. Commun.*, 2011, **2**, 428–432.
28 Z. W. Wang, Y. S. Zhao, K. Tait, X. Z. Liao, D. Schiferl, C. S. Zha, R. T. Downs, J. Qian, Y. T. Zhu and T. D. Shen, *Proc. Natl. Acad. Sci. U. S. A.*, 2004, **101**, 13699–13702.
29 A. Corrias, G. Mountjoy, D. Gozzi and A. Latini, *Nanotechnology*, 2007, **18**, 485610.
30 Z. Wang, D. C. Ba, F. Liu, P. J. Cao, T. Z. Yang, Y. S. Gu and H. J. Gao, *Vacuum*, 2005, **77**, 139–144.
31 A. Anson-Casaos, J. M. Gonzalez-Dominguez, E. Terrado and M. T. Martinez, *Carbon*, 2010, **48**, 1480–1488.
32 B. J. Landi, M. J. Ganter, C. D. Cress, R. A. DiLeo and R. P. Raffaelle, *Energy Environ. Sci.*, 2009, **2**, 638–654.
33 W. Z. Li, C. H. Liang, W. J. Zhou, J. S. Qiu, Z. H. Zhou, G. Q. Sun and Q. Xin, *J. Phys. Chem. B*, 2003, **107**, 6292–6299.
34 W. Feng, X. D. Bai, Y. Q. Lian, J. Liang, X. G. Wang and K. Yoshino, *Carbon*, 2003, **41**, 1551–1557.
35 J. Liu, Y. Zhang, M. Ionescu, R. Y. Li and X. L. Sun, *Appl. Surf. Sci.*, 2011, **257**, 7837–7844.
36 V. G. Pol and M. M. Thackeray, *Energy Environ. Sci.*, 2011, **4**, 1904–1912.
37 D. Abdula, K. T. Nguyen, K. Kang, S. Fong, T. Ozel, D. G. Cahill and M. Shim, *Phys. Rev. B: Condens. Matter Mater. Phys.*, 2011, **83**, 205419.
38 U. J. Kim, C. A. Furtado, X. M. Liu, G. G. Chen and P. C. Eklund, *J. Am. Chem. Soc.*, 2005, **127**, 15437–15445.
39 H. Kim and J. Cho, *Nano Lett.*, 2008, **8**, 3688–3691.
40 X. F. Li, J. Liu, Y. Zhang, Y. L. Li, H. Liu, X. B. Meng, J. L. Yang, D. S. Geng, D. N. Wang, R. Y. Li and X. L. Sun, *J. Power Sources*, 2012, **197**, 238–245.
41 X. F. Li, A. Dhanabalan, X. B. Meng, L. Gu, X. L. Sun and C. L. Wang, *Microporous Mesoporous Mater.*, 2012, **151**, 488–494.
42 X. F. Li and Y. L. Xu, *Electrochem. Commun.*, 2007, **9**, 2023–2026.
43 X. H. Huang, J. P. Tu, B. Zhang, C. Q. Zhang, Y. Li, Y. F. Yuan and H. M. Wu, *J. Power Sources*, 2006, **161**, 541–544.
44 I. Mukhopadhyay, N. Hoshino, S. Kawasaki, F. Okino, W. K. Hsu and H. Touhara, *J. Electrochem. Soc.*, 2002, **149**, A39–A44.
45 J. P. Maranchi, A. F. Hepp and P. N. Kumta, *Electrochem. Solid-State Lett.*, 2003, **6**, A198–A201.
46 S. Ohara, J. Suzuki, K. Sekine and T. Takamura, *J. Power Sources*, 2003, **119–121**, 591–596.
47 J. Morales, L. Sanchez, S. Bijani, L. Martinez, M. Gabas and J. R. Ramos-Barrado, *Electrochem. Solid-State Lett.*, 2005, **8**, A159–A162.
48 S.-W. Song, K. A. Striebel, R. P. Reade, G. A. Roberts and E. J. Cairns, *J. Electrochem. Soc.*, 2003, **150**, A121–A127.
49 T. Moon, C. Kim and B. Park, *J. Power Sources*, 2006, **155**, 391–394.
50 D. W. Liu and G. Z. Cao, *Energy Environ. Sci.*, 2010, **3**, 1218–1237.
51 H. Buqa, D. Goers, M. Holzapfel, M. E. Spahr and P. Novak, *J. Electrochem. Soc.*, 2005, **152**, A474–A481.
52 A. Marschilok, C. Y. Lee, A. Subramanian, K. J. Takeuchi and E. S. Takeuchi, *Energy Environ. Sci.*, 2011, **4**, 2943–2951.
53 H. Zhang, G. P. Cao and Y. S. Yang, *Energy Environ. Sci.*, 2009, **2**, 932–943.
54 S. S. Zhang and T. R. Jow, *J. Power Sources*, 2002, **109**, 422–426.
55 C. Masarapu, V. Subramanian, H. W. Zhu and B. Q. Wei, *Adv. Funct. Mater.*, 2009, **19**, 1008–1014.
56 I. Lahiri, S. M. Oh, J. Y. Hwang, C. Kang, M. Choi, H. Jeon, R. Banerjee, Y. K. Sun and W. Choi, *J. Mater. Chem.*, 2011, **21**, 13621–13626.
57 J. Chen, J. Z. Wang, A. I. Minett, Y. Liu, C. Lynam, H. K. Liu and G. G. Wallace, *Energy Environ. Sci.*, 2009, **2**, 393–396.
58 B. J. Landi, C. D. Cress and R. P. J. Raffaelle, *J. Mater. Res.*, 2010, **25**, 1636–1644.
59 R. Tummala, R. K. Guduru and P. S. Mohanty, *J. Power Sources*, 2012, **199**, 270–277.
60 W. X. Chen, J. Y. Lee and Z. L. Liu, *Carbon*, 2003, **41**, 959–966.